Journal of Inorganic and General Chemistry
ZAAC
Zeitschrift für anorganische und allgemeine Chemie
www.zaac.wiley-vch.de
RESEARCH ARTICLE
Check for updates
DOI: 10.1002/zaac.202300152

Special Issue

Fe_3Mo_3N: Crystal Structure, High-Temperature Behavior, and Catalytic Activity for Ammonia Decomposition

Sophie Hund,[a] Oscar Gómez-Cápiro,[b] Kassiogé Dembélé,[b, c] Stefan Berendts,[a] Thomas Lunkenbein,[c] Holger Ruland,[b] Eva M. Heppke,[a] and Martin Lerch*[a]

Dedicated to Prof. Michael Ruck on the Occasion of his 60th Birthday.

Fe_3Mo_3N was synthesized successfully *via* ammonolysis out of an oxidic precursor prepared by a modified Pechini route. Rietveld refinement using X-ray powder data confirmed that the compound crystallizes in space group $Fd\bar{3}m$ with a lattice parameter of $a = 11.0777$ Å. Group theoretical methods were applied to elucidate the relation between the crystal structure of Fe_3Mo_3N and that of the copper type. The high temperature behavior of Fe_3Mo_3N in ammonia gas was investigated by *in situ* powder X-ray diffraction. In addition, the catalytic activity of our iron molybdenum nitride for ammonia decomposition was measured and compared to the activity of an industrial iron-based catalyst. Both catalysts show similar performances.

Introduction

Hydrogen is deemed to be a promising alternative energy carrier but its transportation is difficult. Intensively studied hydrogen storage molecules are methane and methanol, the latter especially because of its high content of hydrogen (12.6 wt%) and easy handling, but both compounds finally lead to CO_2 emission. A carbon-free alternative is ammonia. It contains 17.6 wt% hydrogen, even more than methanol, and during its decomposition the desired hydrogen and the harmless by-product nitrogen are formed. In addition, ammonia production is a well-established industrial process and already a highly developed ammonia infrastructure exists.[1]

In order to make stored hydrogen useable, ammonia has to be decomposed using a catalyst. A number of materials have already been investigated in this regard, *e.g.* La_2O_3-supported metals such as ruthenium[2] and nickel,[3] WC[4] Mo_2C,[5] and Mo_2N with a large surface area.[6] Also ternary nitrides seem to be promising materials as catalysts for ammonia decomposition: some transition metal molybdenum nitrides are already known to be quite good catalysts, *e.g.* Fe_3Mo_3N and Co_3Mo_3N. Co_3Mo_3N exhibited *ca.* 94% of ammonia conversion at 550 °C, Fe_3Mo_3N showed a slightly lower activity.[7] Our contribution examines the compound Fe_3Mo_3N more closely in relation to its crystal structure, its high-temperature behavior, and the catalytic activity for ammonia decomposition.

[a] *S. Hund, Dr. S. Berendts, Dr. E. M. Heppke, Prof. Dr. M. Lerch*
Institut für Chemie
Technische Universität Berlin
Straße des 17. Juni 135, 10623 Berlin, Germany
E-mail: martin.lerch@tu-berlin.de
[b] *Dr. O. Gómez-Cápiro, Dr. K. Dembélé, Dr. H. Ruland*
Department of Heterogeneous Reactions
Max Planck Institute for Chemical Energy Conversion
Stiftstraße 34–36, 45470 Mülheim an der Ruhr, Germany
[c] *Dr. K. Dembélé, PD Dr. T. Lunkenbein*
Department of Inorganic Chemistry
Fritz-Haber-Institut der Max-Planck-Gesellschaft
Faradayweg 4–6, 14195 Berlin, Germany

Special Issue *This article is part of a Special Collection dedicated to Professor Michael Ruck on the occasion of his 60th birthday. Please see our homepage for more articles in the collection.*

Results and Discussion

Chemical Characterization. Iron molybdenum nitride Fe_3Mo_3N was synthesized successfully – using an oxide precursor (see Experimental Section) – as phase-pure black powder with metallic glance. The desired iron to molybdenum ratio in the final product is 1:1 which is proofed by means of energy dispersive X-ray spectroscopy – resulting in a ratio of Fe:Mo = 1.002:1.000.

Fe_3Mo_3N was structurally characterized by powder X-ray diffraction. It is not possible to distinguish between oxygen and nitrogen using this method. Hot gas extraction measurements were performed to determine the anion content. This resulted in an oxygen amount of 1.51% and a nitrogen content of 3.11% (calculated: 0% for oxygen, 2.98% for nitrogen) – this corresponds to the molecular formula $Fe_3Mo_3N_{1,06}O_{0,45}$. The measured nitrogen amount well fits to the theoretical value. However, some oxygen was also observed which will be discussed later. Nevertheless, for reasons of simplicity, the compound will be called Fe_3Mo_3N furthermore.

Crystal Structure. The structural refinement of Fe_3Mo_3N, which crystallizes in space group $Fd\bar{3}m$, was done applying the Rietveld[8] method using the coordinates reported by Jackson et al.[9] as starting values. Figure 1 shows the diffraction pattern of Fe_3Mo_3N with the results of the Rietveld refinement. The

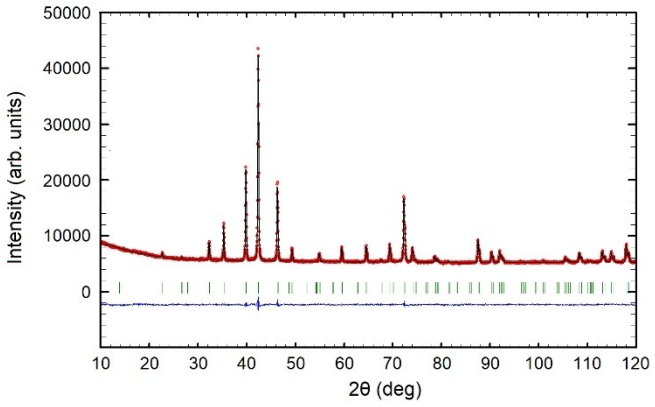

Figure 1. Powder X-ray diffraction pattern of Fe_3Mo_3N with the results of the Rietveld refinement (red: measured, black: calculated, green: reflection positions, blue: difference plot).

corresponding structure type is that of Fe_3W_3C, also called η-carbide type. A description of this structure type as filled Ti_2Ni structure can be found too.[10,11] The cell parameter is a = 11,0777 Å and 16 formular units are in the unit cell, further details of the results of the Rietveld refinement are given in Table 1. Table 2 shows the refined atomic parameters and Debye–Waller factors.

The anions occupy Wyckoff position 16*c*. Iron is located on two distinct sites, 16*d* and 32*e*, respectively, whereas molybdenum can be found on a 48*f* position. It should be mentioned that the group-subgroup discussion presented below, elucidating the structural relationship between the copper type and Fe_3Mo_3N, shows that there are two types of voids at positions 96*h* and 48*f*, respectively. The above-mentioned excess anions could occupy these voids. This assumption was tested by evaluation of the calculated difference Fourier maps. Such a kind of analysis did not give any hint concerning excess atoms on these positions. Unfortunately, Jackson et al.[9] did not determine the oxygen content. Our structural parameters are in good agreement with the values reported by them. They published a lattice parameter of a = 11.0859 Å (this work: 11.0777 Å) and our atomic coordinates deviate imperceptibly from their values.

In order to investigate the reason for the measured oxygen excess, STEM-EELS (scanning transmission electron microscope and electron energy loss spectroscopy) measurements were carried out. These images show the presence of agglomerates that consist of elongated particles (Figure 2a). In addition, a thin surface layer (Figure 2b) with a thickness of *ca.* 2.4–3.0 nm has been observed encapsulating the particles. Chemical analyses by STEM-EELS measurements (Figure 2c) point to the presence of oxygen in the layer (in addition to Fe and Mo – the N–K- and Mo–M_3-edge are overlapping) but not in the bulk.

Due to the fact that oxygen is located at the surface of the particles (probably an amorphous surface layer), it is not relevant for Rietveld refinement.

Table 1. Results of the Rietveld refinement for Fe_3Mo_3N (standard deviations in parenthesis).

	Fe_3Mo_3N
Space group	$Fd\bar{3}m$ (No. 227)
Structure type	Fe_3W_3C
Z	16
a/Å	11.0777(3)
V/Å^3	1359.36(6)
ρ_{calc}/g cm^{-3}	9.174
Diffractometer	PANalytical X'Pert Pro
Radiation	Cu–Kα (wavelengths: 1.54056 Å, 1.54439 Å)
R_p	0.0108
R_{wp}	0.0138
R_{exp}	0.0129
R_{Bragg}	0.0377
S	1.07

Table 2. Refined atomic parameters for Fe_3Mo_3N (standard deviations in parenthesis).

Atom	Wyckoff	x	y	z	B_{iso}/Å^2
Fe1	32*e*	0.29399 (13)	0.29399 (13)	0.29399 (13)	0.58(8)
Fe2	16*d*	1/2	1/2	1/2	0.47(11)
Mo	48*f*	0.32182(11)	1/8	1/8	0.43(5)
N/O	16*c*	0	0	0	1*

* Not refined.

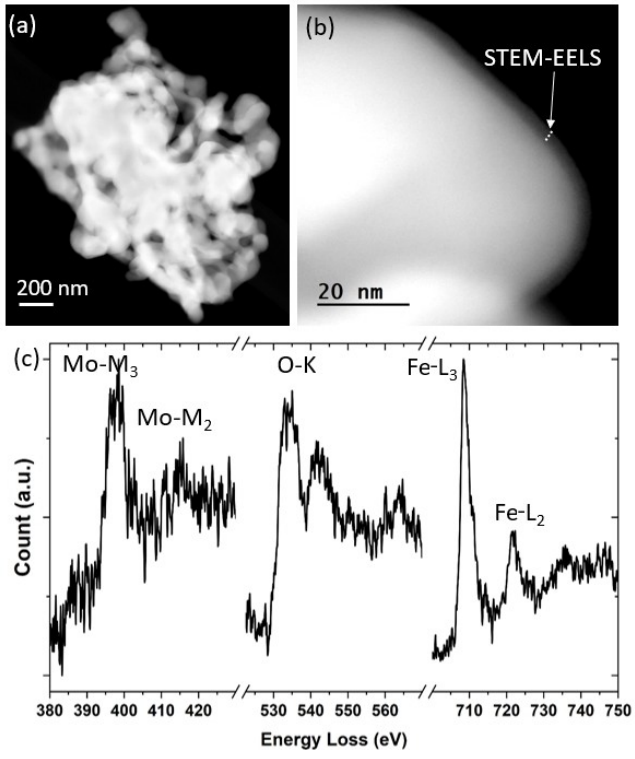

Figure 2. STEM-EELS images of Fe_3Mo_3N with (a) STEM image of agglomerates, (b) the layer containing oxygen, and (c) chemical analysis of the layer.

The unit cell of η-carbide-type Fe_3Mo_3N is shown in Figure 3. The (NMo_6)-octahedra are corner-shared in the presented way. Interestingly, nitrogen is exclusively surrounded by molybdenum. Bem et al.[12] described not only connected (NMo_6)-octahedra but also mentioned ($Fe[Mo_6Fe_6]$)- and ($Fe[Mo_6Fe_4N_2]$)-pseudo-icosahedra. The name is coming from the fact that the described polyhedra are strongly distorted compared to ideal icosahedra. Furthermore, the central atom (Fe) is surrounded by two or three different species (Fe, Mo, and N) to build the polyhedra, which is quite unusual. A description of this structure as two interpenetrating diamondoid subunits has also been reported[11] but this is not considered in detail here.

Looking at the parameters and the coordination spheres of the metal atoms (shown in Figure 4), the following can be stated: Fe1 is surrounded by six molybdenum atoms, three Fe1 atoms, and three Fe2 atoms, resulting in ($Fe[Mo_6Fe_6]$)-'icosahedra'. The polyhedra around Fe2 are built up of six Mo atoms and six Fe1 atoms corresponding to the described 'pseudo-icosahedra' ($Fe[Mo_6Fe_6]$) by Bem et al.[12] A $Fe[Mo_6Fe_4N_2]$-icosahedron could not be found, instead we visualize ($Mo[Mo_4Fe_6N_2]$)-'icosahedra' consisting of 4 Fe1, 2 Fe2, 4 Mo, and 2 N atoms (see Figure 4), exhibiting large differences in the individual distances of the coordinating atoms to the central molybdenum.

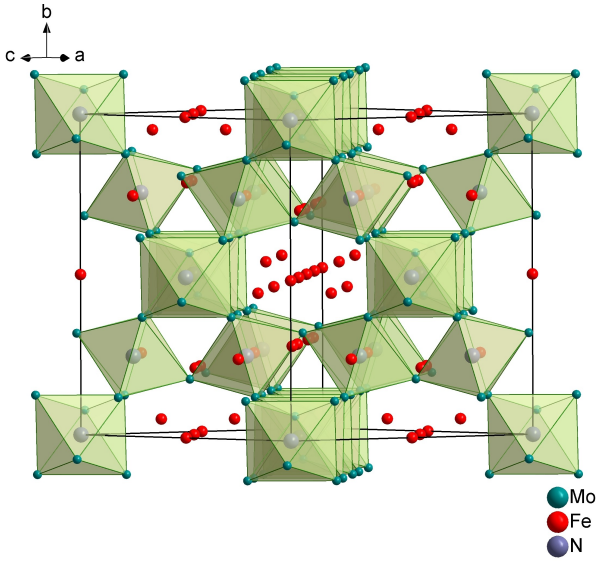

Figure 3. Unit cell of Fe_3Mo_3N (Fe_3W_3C-type structure) with (NMo_6)-octahedra; Fe atoms in red, Mo atoms in petrol and N atoms in blue-grey, the polyhedra are green colored.

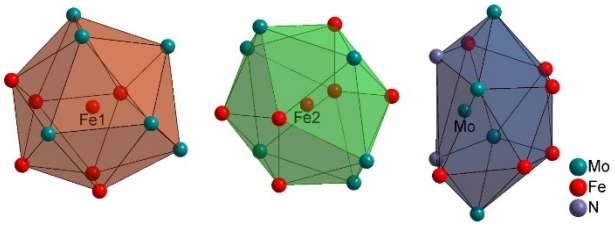

Figure 4. Coordination spheres around Fe1 (red), Fe2 (green), and Mo (blue) in Fe_3Mo_3N.

In Table 3, the interatomic distances in Fe_3Mo_3N are listed (up to 3 Å) and compared to the values for Fe_3W_3N. The Fe1–Fe1 distances are slightly shorter than the reported value of 2.559 Å for Fe_3W_3N. In contrast, the other values are almost identical to each other. Consequently, there is no strong effect on the distances due to substitution of tungsten by molybdenum.

To get a deeper understanding of the crystal structure of Fe_3Mo_3N, its relationship to a simple structure type with high symmetry was evaluated using group theoretical concepts.[14] The Bärnighausen tree[15] in Figure 5 shows the group-subgroup relations between the cubic closest packed Cu-type and the Fe_3W_3C-type structure adopted by Fe_3Mo_3N. Starting from space group $Fm\bar{3}m$ for the Cu-type, *via* a *klassengleiche* transition with index 4 (k4), the Cu_3Au-type structure with space group $Fd\bar{3}m$ is reached. The 4*a* site splits to an 1*a* site, occupied by Au, and a 3*c* site, occupied by Cu in Cu_3Au. The following symmetry reduction through another *klassengleiche* transition of index 4 (k4) and a doubling of the lattice parameters lead to space group $Im\bar{3}m$, where the 3*c* site splits to 12*d* and 12*e*. The next *klassengleiche* transition of index 2 (k2) results in space group $Pn\bar{3}m$ (origin choice 2), whereat the 8*c* site splits to a 4*b* site and a 4*c* site. In the final step there is again a *klassengleiche* transition with index 2 (k2) and the unit cell is enlarged for the second time by doubling the lattice parameter leading to the Fe_3W_3C-type structure with space group $Fd\bar{3}m$ (origin choice 2) which is adopted by Fe_3Mo_3N with Fe1 on Wyckoff position 32*e*, Fe2 on 16*d*, and the anions on 16*c* resulting from the splitting of the 4*c* site as just mentioned. Mo occupies the 48*f* site and two unoccupied positions 48*f* and 96*h* occur.

Overall, there is a good accordance of calculated and refined atom positions, even if there are some aberrations. Especially molybdenum is disarranged in relation to its *x* value. It should be around 0.25 (calculated) but it is ~0.32 in Fe_3Mo_3N. The iron atoms are slightly displaced as well. These differences lead to the description of the metal polyhedra as 'distorted icosahedra' in literature, which is at first glance not convincing in consideration to the fact that the copper type has a cubic closest packing, where cuboctahedra are present.

Table 3. Selected interatomic distances in Fe_3Mo_3N compared to Fe_3W_3N (in Å, standard deviations in parenthesis).

	Fe_3Mo_3N	Fe_3W_3N[13]
Fe1–Fe1	2.538(2) [3×]	2.559(7) [3×]
Fe1–Fe2	2.3837(15) [3×]	2.393(7) [3×]
Fe1–Mo/W	2.7690(15) [3×]	2.777(4) [3×]
Fe1–Mo/W	2.6653(16) [3×]	2.666(7) [3×]
Fe2–Fe1	2.3837(15) [6×]	2.393(7) [6×]
Fe2–Mo/W	2.7804(6) [6×]	2.789(7) [6×]
Mo/W–Fe1	2.7690(15) [2×]	2.777(4) [2×]
Mo/W–Fe1	2.6653(16) [2×]	2.666(7) [2×]
Mo/W–Fe2	2.7804(6) [2×]	2.789(7) [2×]
Mo/W–N	2.1137(8) [2×]	2.119(5) [2×]
Mo/W–Mo/W	2.8920(3) [4×]	2.901(2) [4×]
N–Mo/W	2.1137(8) [6×]	2.119(5) [6×]

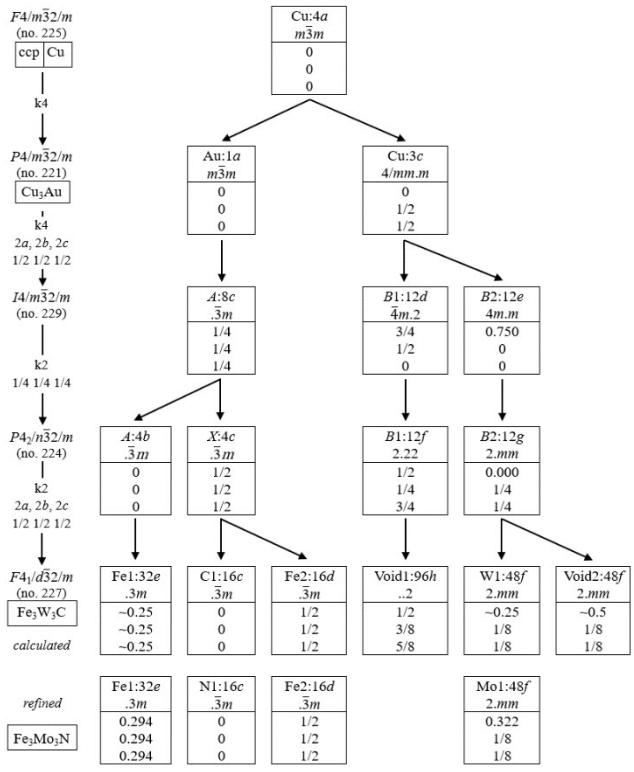

Figure 5. Bärnighausen tree for the group-subgroup relation between the Cu-type and the crystal structure of the Fe_3W_3C-type.

***In situ* X-ray diffraction**. Srifa et al.[7] already performed measurements on the catalytic activity of Fe_3Mo_3N as catalyst for ammonia decomposition. They also showed X-ray diffraction patterns before and after the catalytic measurements. In the latter case, there was no more Fe_3Mo_3N observed but MoN and Fe_2N (catalyst decomposition). In order to understand this observation in more detail, *in situ* powder X-ray diffraction measurements were carried out. Fe_3Mo_3N was annealed in temperature steps of 50 °C (10.0 K min^{-1}) under flowing ammonia gas (120 mL min^{-1}). The relevant data, up to 600 °C, is shown in Figure 6 – this is the maximum temperature at which the following catalytic measurements have been carried out. At around 450 °C, the ternary nitride decomposes (and reacts) to the binary nitrides MoN and Fe_2N. At 500 °C, it is completely decomposed. Thus, the catalytic active material is most likely not Fe_3Mo_3N but one or both binary metal nitrides.

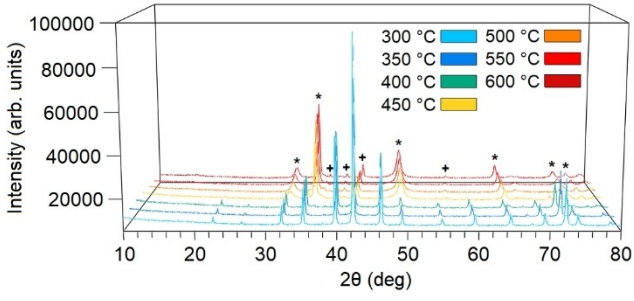

Figure 6. *In situ* X-ray diffraction patterns of our Fe_3Mo_3N sample up to 600 °C. Each color is assigned to a certain temperature indicated in the table (* = MoN, + = Fe_2N).

The following section deals with the catalytic activity of our prepared Fe_3Mo_3N sample. Due to the oxygen containing layer on the particle surface, a pretreatment procedure at 400 °C was applied (see Experimental Section).

Catalytic measurements. Figure 7 shows the conversion of ammonia to N_2 and H_2 in the range of 400 to 600 °C tested for our prepared Fe_3Mo_3N and, for comparison, an industrial Fe-based catalyst as reference. Both materials show a more or less similar behavior with a strong increase in ammonia conversion at temperatures above 500 °C. While the industrial reference catalyst shows a slight deactivation, observable in a lower conversion at 550 °C for the value obtained in the second part of the experiment while cooling down to 400 °C, which is most likely due to some initial surface restructuration during reaction conditions, our prepared Fe_3Mo_3N did not exhibit any deactivation over the whole range of the activity test. Interestingly, the irreversible decomposition of Fe_3Mo_3N at around 450 °C is not reflected in the catalytic activity. This might due to the fact that both Fe-based catalysts exhibit a reasonable activity under the conditions applied only at temperatures above those at which the decomposition was observed. Further studies are required to elucidate the instability of the Fe_3Mo_3N and to be able to distinguish the contribution of the binary phases to the activity. The obtained results are in line with conversion data reported in literature[7] for Fe–Mo-based materials. Fe-based catalysts are beside other transition metal-based catalysts like Ni and Co the most discussed candidates for ammonia decomposition, showing an encouraging activity compared to the frequently studied catalysts based on the precious metal Ru.[1d,16] As the performance of our Fe_3Mo_3N can compete with the data reported in

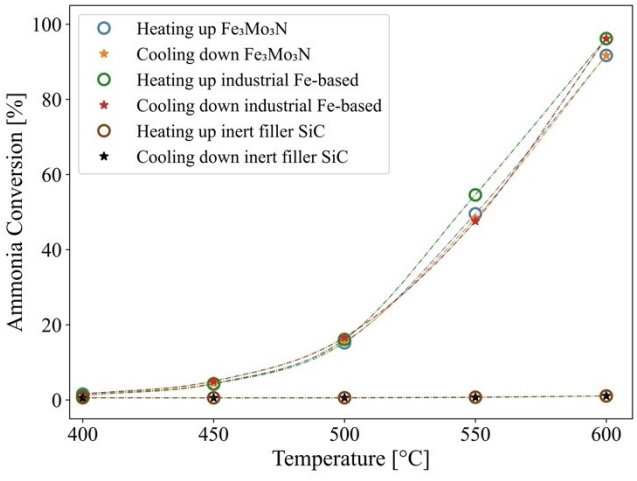

Figure 7. Activity of Fe_3Mo_3N and an industrial Fe-based catalyst as reference for the decomposition of ammonia in a temperature range between 400 °C and 600 °C. Reaction conditions: p = 1 atm, flow rate = 0.6 ml mg_{cat}^{-1} min^{-1}, rate of temperature change between the steps = 2.5 °C min^{-1}.

literature this material is a promising starting point for further fundamental studies in ammonia decomposition, *e.g.* to examine the effects of promotors.

Conclusions

Fe_3Mo_3N (space group $Fm\bar{3}m$, $a = 11.0777$ Å) was successfully synthesized and characterized. A group theoretical approach elucidates a relation between the Cu-type (aristotype, $Fm\bar{3}m$) and the crystal structure of Fe_3Mo_3N. The high temperature behavior was investigated by *in situ* powder X-ray diffraction and shows a decomposition by reaction with ammonia gas to MoN and Fe_2N starting at around 450 °C. The catalytic activity for ammonia decomposition showed an activity similar to that of an industrial Fe-based catalyst (Clariant International Ltd, Switzerland). So far, no optimization strategies were applied for Fe_3Mo_3N (particle size, morphology, promotors etc.). Consequently, the activity can most likely be enhanced. More details concerning the catalytic properties (kinetics etc.) and quaternary materials derived from Fe_3Mo_3N will be presented in forthcoming contributions.

Experimental Section

Synthesis. On the basis of nitrides prepared in our group, *e.g.* $TaZrN_3$[17] and $Eu_2Ta_2(O,N)_{7+\delta}$,[18] the Pechini[19] route was used to prepare an oxidic precursor. Iron(III) nitrate nonahydrate (Merck) and citric acid (≥ 99.5 %, Merck) were dissolved in an absolute ethanol-water-mixture with ratio 1 : 1 to receive an iron citrate solution. For the corresponding molybdenum solution, citric acid was dissolved in absolute ethanol and this solution was added drop by drop to molybdenum(V) chloride (99.99 %, Sigma Aldrich). In both cases, citric acid was used in a 12-fold excess compared to the metal ion. Afterwards the solutions were mixed in the desired ratio and an excess of ethylene glycol was added. The solvents were evaporated by stepwise heating and a gel was formed which was calcinated at 450 °C for approximately 16 h. This procedure yielded mixed-metal oxides which were used as precursors. The oxides were transformed to nitrides by ammonolysis in a tube furnace at 875 °C with an ammonia flow of 9 Lh^{-1} and a total holding time up to 40 h. The furnace was cooled down under flowing nitrogen.

Chemical and structural characterization. STEM-EDX analysis was conducted in a FEI Talos F200X microscope operating at 200 kV. The contents of nitrogen and oxygen were measured by hot gas extraction with a LECO TC-300/EF-300 N/O analyzer with ZrO_2 and steel as standard materials – the standard deviation is estimated at 2 %. A PANalytical X'Pert Pro powder diffractometer (operating in a Bragg-Brentano set-up) with nickel-filtered Cu–Kα radiation was used for the powder X-ray diffraction measurements. The data was collected at ambient temperature over an angular range of 10–120° and a step size of 0.026°. Rietveld refinement was executed with the program package FullProf Suite 2021.[20] STEM-EELS was investigated on a JEOL ARM 200F operating at 200 kV. This microscope is equipped with a cold field-emission gun (FEG) and a dual spherical aberration (Cs) corrector and Gatan image filter (Quantum) which allow the study of the morphology and structure of the sample by high-resolution scanning TEM (HR-STEM) and electron energy loss spectroscopy (EELS).

***In situ* powder X-ray diffraction.** For *in situ* powder X-ray diffraction measurements, a Rigaku SmartLab 3 kW system operating in a Bragg-Brentano set-up with nickel-filtered Cu–Kα radiation equipped with a Reactor X was used. The measurements were carried out over an 2θ range of 10–80° with a step size of 0.020°. The reactor was heated up in steps of 50 °C with a heating rate of 10.0 ± 0.1 K min^{-1}. The temperature is kept constant for a measurement of 28 minutes before heating up to the next stage. The gas atmosphere was ammonia (quality 3.8, Air Liquide) with a flow rate of 120 ± 10 mL min^{-1}.

Activity test on decomposition of ammonia. The catalytic activity of our prepared Fe_3Mo_3N was tested in a fixed-bed reactor. 200 mg of the catalyst were diluted in a mass ratio of 1 : 2 with SiC. The catalysts particle size was 200–300 μm, while the SiC particle size was 300–400 μm to enable a later separation of the spent catalyst from the dilution material. The test procedure started with a pretreatment, heating the sample with a rate of 1 °C min^{-1} in nitrogen (quality 5.0) up to 400 °C applying a flow rate of 1 ml mg_{cat}^{-1} min^{-1}. The gas feed was then switched to ammonia (quality 5.0) with a flow rate of 0.6 ml mg_{cat}^{-1} min^{-1}. After 60 min at 400 °C the temperature was increased in steps of 50 °C to 600 °C and back to the initial temperature, whereas for each step the temperature was kept constant for 60 min. The rate of temperature change was 2 °C min^{-1}. For comparison, an industrial Fe-based catalyst was tested under similar conditions, but with a reductive pretreatment according to the manufacturer. In addition, a test was made filling the reactor only with SiC following the same program of temperature and flow. Product gas analysis was performed *via* IR detectors for quantification of NH_3 and H_2O as well as a TCD for H_2 (Emerson XStream XEGP).

Acknowledgements

We thank the Federal Ministry of Education and Research, Germany (Bundesministerium für Bildung und Forschung, BMBF, Verbundvorhaben TransHyDE Forschungsverbund AmmoRef, supportcodes: 03HY203C, 03HY203A), for funding. The industrial reference catalyst used in this study was kindly provided by our project partner Clariant. This work was also supported by the Deutsche Forschungsgemeinschaft (INST 131/734-1 FUGG). Open Access funding enabled and organized by Projekt DEAL.

Conflict of Interest

The authors declare no conflict of interest.

Data Availability Statement

The data that support the findings of this study are available from the corresponding author upon reasonable request.

Keywords: nitrides · ammonia decomposition · group-subgroup relation · *in situ* X-ray diffraction · catalysis

[1] a) F. Schüth, R. Palkovits, R. Schlögl, D. S. Su, *Energy Environ. Sci.* **2012**, *5*, 6278–6289; b) A. Klerke, C. H. Christensen, J. K. Nørskov, T. Vegge, *J. Mater. Chem.* **2008**, *18*, 2304–2310; c) J. Kothandaraman, S. Kar, R. Sen, A. Goeppert, G. A. Olah, G. K. S. Prakash, *J. Am. Chem. Soc.* **2017**, *139*, 2549–2552; d) S. Ristig, M. Poschmann, J. Folke, O. Gómez-Cápiro, Z. Chen, N. Sanchez-Bastardo, R. Schlögl, S. Heumann, H. Ruland, *Chem. Ing. Tech.* **2022**, *94*, 1413–1425.
[2] C. Huang, Y. Yu, J. Yang, Y. Yan, D. Wang, F. Hu, X. Wang, R. Zhang, G. Feng, *Appl. Surf. Sci.* **2019**, *476*, 928–936.
[3] H. Muroyama, C. Saburi, T. Matsui, K. Eguchi, *Appl. Catal. A* **2012**, *443 (444)*, 119–124.
[4] S. S. Pansare, W. Torres, J. G. Goodwin Jr., *Catal. Commun.* **2007**, *8*, 649–654.
[5] J.-G. Choi, *J. Ind. Eng. Chem.* **2004**, *10*, 967–971.
[6] S. Podila, S. F. Zaman, H. Driss, Y. A. Alhamed, A. A. Al-Zahrani, L. A. Petrov, *Catal. Sci. Technol.* **2016**, *6*, 1496–1506.
[7] a) A. Srifa, K. Okura, T. Okanishi, H. Muroyama, T. Matsui, K. Eguchi, *Catal. Sci. Technol.* **2016**, *6*, 7495–7504; b) S. F. Zaman, L. A. Jolaloso, A. A. Al-Zahrani, Y. A. Alhamed, S. Podila, H. Driss, M. A. Daous, L. A. Petrov, *Bulg. Chem. Commun.* **2018**, *50*, 181–188.
[8] H. M. Rietveld, *J. Appl. Cryst* **1969**, *2*, 65–71.
[9] S. K. Jackson, R. C. Layland, H.-C. zur Loye, *J. Alloys Compd.* **1999**, *291*, 94–101.
[10] A. Westgren, *Jernkont. Ann.* **1933**, *117*, 1.
[11] T. J. Prior, P. D. Battle, *J. Mater. Chem.* **2004**, *14*, 3001–3007.
[12] D. S. Bem, C. P. Gibson, H.-C. zur Loye, *Chem. Mater.* **1993**, *5*, 1993.
[13] K. S. Weil, P. N. Kumta, *Actra Cryst.* **1997**, *C53*, 1745–1748.
[14] a) M. I. Aroyo, J. M. Perez-Mato, C. Capillas, E. Kroumova, S. Ivantchev, G. Madariaga, A. Kirov, H. Wondratschek, *Z. Kristallogr.* **2006**, *221 (1)*, 15–27; b) S. Ivantchev, E. Kroumova, G. Madariaga, J. M. Pérez-Mato, M. I. Aroyo, *J. Appl. Crystallogr.* **2000**, *33*, 1190–1191.
[15] H. Bärnighausen, *MATCH Commun. Math. Comput. Chem.* **1980**, *9*, 139–175.
[16] I. Lucentini, X. Garcia, X. Vendrell, J. Llorca, *Ind. Eng. Chem. Res.* **2021**, *60*, 18560.
[17] T. Lüdtke, S. Orthmann, M. Lerch, *Z. Naturforsch.* **2017**, *72(4)b*, 305–311.
[18] B. Anke, S. Hund, C. Lorent, O. Janka, T. Block, R. Pöttgen, M. Lerch, *Z. Anorg. Allg. Chem.* **2017**, *643*, 1824–1830.
[19] M. R. Pechini, *US Pat. No. 3,330,697*, **1967**.
[20] R. Rodríguez-Carvajal, FULLPROF, A program for Rietveld refinement and pattern matching analysis. *In Satellite Meeting on Powder Diffraction of the 15th International Congress of the IUCr, Toulouse (France)* **1990**, p. 127.

Manuscript received: July 5, 2023
Revised manuscript received: August 29, 2023

